33rd Annual International Conference of the IEEE EMBS
Boston, Massachusetts USA, August 30 - September 3, 2011

Venous Vessel Boundary Delineation at High Field Using Sigmoid-SWI

Amanda Ng, Gary F. Egan, Zang-Hee Cho and Leigh A. Johnston

***Abstract*— Susceptibility Weighted Imaging (SWI) is an increasingly utilised MRI technique for enhancing image contrast by attenuating magnitude data with a mask derived from the phase data. It is particularly useful for venography, however at higher field strengths, the effects of localised magnetic susceptibility differences lead to ill-defined edges within SWI images and overestimation of widths in large veins oriented perpendicular to the main field. We propose a variation on SWI, sigmoid-SWI, that removes the vessel boundary artefacts, resulting in clearer visibility of edges and more accurate widths of venous vessels.**

I. Introduction

Susceptibility Weighted Imaging [1], [2] is a magnetic resonance imaging (MRI) method that combines information in the magnitude and phase of the acquired data to produce images with enhanced contrast. The method involves creation of a phase mask that is used to attenuate voxel intensities in the magnitude image, where the phase mask is either positive (attenuating only voxels whose phase is positive) or negative (attenuating voxels whose phase is negative). Negative phase mask SWI is particularly useful for venography, since the magnetic susceptibility of venous blood and partial volume effects lead to negative phase values. At higher field strengths, the effects of localised magnetic susceptibility differences are amplified, leading to increased phase contrast and larger susceptibility artefacts [3], [4]. For larger veins that are oriented perpendicular to the direction of the main field, the susceptibility difference between the vein and surrounding tissue causes dipolar changes in the magnetic field immediately outside the vein. The field changes result in increased phase in the plane perpendicular to the main field, decreased phase in the direction parallel to the main field and magnitude attenuation. In SWI, this can affect the visibility of the large vein boundaries, resulting in incorrect vessel segmentation, as we will demonstrate. We propose a modification to the SWI phase mask that corrects the vessel boundaries by using the increased phase outside the vessel to amplify the attenuated magnitude.

II. Theory

Physical origins of signal loss surrounding veins at high field

Venous vessels can be modelled as long cylinders whose effects on the surrounding magnetic field is described by [5]

$$\Delta B\left(r,\theta\right)=\frac{\Delta\chi}{2}\sin^{2}\left(\beta\right)\left(\frac{a}{r}\right)^{2}\cos\left(2\theta\right)B_{0}, \qquad (1)$$

where $\Delta\chi$ is the difference in susceptibility between the cylinder and the surrounding tissues, β is the angle between the cylinder and the direction of the main B field, a is the radius of the cylinder and B_0 is the strength of the main B field (Fig. 1a). r and θ are coordinates of a point $\mathbf{r}$ in the plane normal to the cylinder axis, where r is the distance from the cylinder axis to $\mathbf{r}$ and θ is the angle between the direction of the main B field and $\mathbf{r}$ (Fig. 1b). In axial slices, where the vein is perpendicular to the main B field, $\theta=\frac{\pi}{2}$ and $\beta=\frac{\pi}{2}$, the magnitude of ΔB is greatest and ΔB opposes the direction of the main B field.

The phase,

$$\phi=-\gamma\Delta B.T_{E}, \qquad (2)$$

where $\gamma=267.513$ rad.s^{-1}T^{-1} is the gyromagnetic ratio of the H^1 proton and T_E is the echo time, implies that voxels surrounding veins will have positive phase. The product $\gamma\Delta B$ describes the shift in Larmor frequency resulting from the cylinder. At $B_0=7$ T, typical acquisition bandwidth per voxel is 30 Hz, corresponding to $\Delta B\approx0.7\times10^{-6}$ T. The susceptibility of deoxygenated blood in venous vessels is $\Delta\chi\approx1.6$ ppm [6]. The largest field shifts occur in the voxels adjacent to the vein, that is, $r_A=a+w$, where w is the width of a voxel. Substitution of these values into (1) results in $\frac{a}{a+w}=0.37$. The minimum vein radius required to produce a frequency shift large enough to cause a one voxel spatial shift of protons at position $\left(r_A,\frac{\pi}{2}\right)$, and therefore substantially affect the magnitude intensity, is $R_{min}=\frac{a}{w}=0.58$, where R_{min} is a fraction of the voxel width.

Susceptibility Weighted Imaging

SWI is calculated voxel-wise from the magnitude and phase data as

$$S\left(\mathbf{v}\right)=\rho\left(\mathbf{v}\right)F\left(\mathbf{v}\right)^{n} \qquad (3)$$

where $S\left(\mathbf{v}\right)$ is the intensity in the SWI image of voxel $\mathbf{v}$, $\rho\left(\mathbf{v}\right)$ is the magnitude of the voxel, n is an exponent,

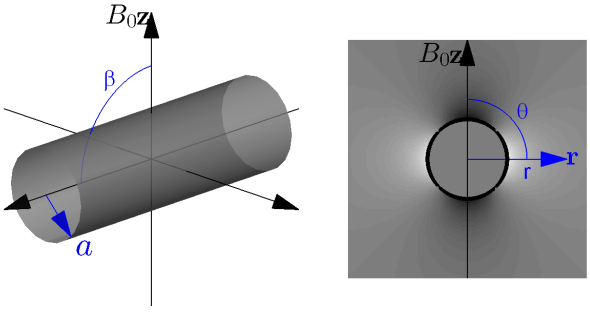

(a) (b)

Fig. 1: Parameter definitions for deriving the change in B field outside (a) a cylinder perpendicular to the main field and (b) the change in B field produced by this cylinder.

typically chosen as $n = 4$ [1], and $F(\mathbf{v})$ is the phase mask. The positive phase mask is defined as

$$F_+(\mathbf{v}) = \begin{cases} 1, & \phi(\mathbf{v}) < 0 \\ \frac{\pi - \phi(\mathbf{v})}{\pi}, & \phi(\mathbf{v}) \geq 0 \end{cases} \quad (4)$$

and the negative phase mask is defined as

$$F_-(\mathbf{v}) = \begin{cases} \frac{\pi + \phi(\mathbf{v})}{\pi}, & \phi(\mathbf{v}) \leq 0 \\ 1, & \phi(\mathbf{v}) > 0 \end{cases} \quad (5)$$

where $\phi(\mathbf{v})$ is the phase intensity of the voxel. A negative shift will occur in the phase of voxels containing veins provided the spatial resolution in the direction of the main B field is lower than the resolutions in the transverse plane [7]. Although the shift may be visually imperceptible in the phase image, the SWI method is successful at increasing the visibility of veins of subvoxel diameter. However, the attenuation in the magnitude image due to veins parallel to the main B field and having radius larger than R_{min} is not addressed by SWI. This signal loss in voxels surrounding the veins results in blurred vessel edges and a widened appearance of veins. Without correction of the attenuation, overestimation of vessel width will occur.

III. Method

Our proposed modified phase mask, $F_S(\mathbf{v})$, compensates for the attenuation of the magnitude surrounding large veins while maintaining the general contrast of conventional SWI. This is achieved by applying a sigmoid filter to voxels whose phase is less than zero and/or whose magnitude is less than the local gaussian average of non-brain voxels:

$$F_S(\mathbf{v}) = \begin{cases} \frac{2}{1+e^{-k\phi(\mathbf{v})}} & , \phi(\mathbf{v}) \leq 0 \text{ or } \rho(\mathbf{v}) < \rho_t(\mathbf{v}) \\ 1 & , \text{otherwise} \end{cases} \quad (6)$$

where $k = 2.15$ is a constant chosen such that F_S simulates F_-^4 when $\phi(\mathbf{v}) \leq 0$ (Fig. 2). $\rho_t(\mathbf{v})$ is the local average intensity of brain voxels in the magnitude data, calculated as

$$\rho_t(\mathbf{v}) = \left(\frac{(\boldsymbol{\rho} \cdot \mathbf{M}) * \mathbf{G}}{\mathbf{M} * \mathbf{G}} \right)_{\mathbf{v}} \quad (7)$$

where $\boldsymbol{\rho}$ is the magnitude map, $\mathbf{M}$ is a brain/non-brain mask where the value 0 indicates non-brain and 1 indicates brain, $\mathbf{G}$ is a Gaussian window kernel, $\cdot$ indicates voxel-wise multiplication and $*$ indicates the convolution operation. The modified phase mask has a similar attenuation profile to the F_-^4 when phase is negative, but demonstrates amplification properties when phase is positive and the magnitude is below ρ_t (Fig. 2).

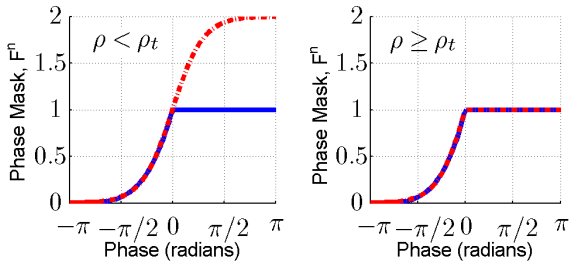

Fig. 2: Comparison of (blue) SWI phase mask, F_-^4, and (red) sigmoid-SWI phase mask, F_S.

Experimental data

MRI data was acquired on a 7T Siemens system with an 8 channel transmit-receive head coil (Neuroscience Research Institute, Incheon, South Korea). Axial T2*-weighted gradient echo (GRE) images were acquired with TE = 21.6 ms, TR = 750 ms, FA = 30°, bandwidth = 30 Hz per pixel, slice thickness = 2mm, FOV = 256 × 224 mm^2 , matrix size = 1024 × 896, spatial resolution was 0.25 × 0.25 × 2 mm^3, a total of 17 slices and total scan time of 11.5 min. Magnitude and wrapped phase data were reconstructed using the optimised complex reconstruction method [8]. Phase was unwrapped using PhUN [9] and background field removed using a spatially dependent filtering method [10]. The Gaussian window kernel in (7) was set to 50 voxels wide with a standard deviation of 10 voxels. The brain/non-brain mask was calculated using active-snake contours [11].

Line profiles from the magnitude, phase, SWI, and sigmoid-SWI image were taken from three regions of interest (ROI) containing vessels oriented perpendicular to the main field. True vessel boundaries were localised at the transitions between positive and negative phase. In the SWI and sigmoid-SWI image, the intensity mean along the line profiles was calculated, excluding voxels designated as vessels in the phase profile. The apparent vessel boundaries in the SWI and sigmoid-SWI were then localised at the transitions below and above the mean.

IV. Results and Discussion

The effects of the high field strength on magnitude and phase intensity surrounding large veins is visible in the acquired data (Fig 3a and 3b). The magnitude image demonstrates attenuation in voxels immediately surrounding large veins that are oriented perpendicular to the main magnetic field, while the phase image demonstrates higher phase values surrounding these veins, as seen in the line profiles in Fig. 4.

The true vessel width, as derived from the phase, is 3 voxels for the yellow ROI and 4 voxels for the blue ROI (red vertical lines, Fig. 4). The estimation of the vessel width assumes that phase values within the voxel will be negative and immediately outside the voxel will be positive, a result of the susceptibility effects described by (1). The estimation does not take into account partial volume effects which are difficult to model, due to the quadratic nature of the change in B field, the non-linearity of phase averaging, the anisotropy of the voxel dimensions and the unknown positioning of the vessel with respects to the voxel limits. Nevertheless, it is reasonable to assume the vessel border will occur within the region comprising adjacent positive and negative phase voxels.

The SWI image (Fig 3c) demonstrates attenuated values immediately outside the veins. The line profiles (Fig. 4)

demonstrate weaker vessel edges compared to the phase profile. Estimation of the boundary of the vessels from the SWI data is complicated by these gradients. Venography derived from SWI employ minimum intensity projection (mIP) techniques under the assumption that vein voxels have lower intensities than non-venous voxels. A similar assumption is made in this paper for localising the boundary of the vessels: vein voxels are assumed to have an intensity below the mean of non-venous voxels. Using this assumption, vessel widths of 5 and 7 voxels are derived for the yellow and blue ROIs, respectively (Fig 4, green arrows), and are 2 and 3 voxels greater than the phase-derived vessel widths.

The sigmoid-SWI image (Fig 3d) is overall similar to the SWI. However, on closer examination, the sigmoid-SWI produces more accurate vessel delineation, as follows. The sigmoid-SWI line profiles (Fig. 4) have steeper gradients than the SWI profiles and corrected vessel widths are 3 and 4 voxels for the yellow and blue ROIs, respectively (Fig 4, purple arrows), in agreement with vessel widths derived from the phase.

The implementation of the local average threshold, ρ_t, ensures that the sigmoid-SWI image maintains the general contrast of SWI. Omitting the threshold and applying the sigmoid filter over all voxels results in intensity increases in voxels with positive phase (Fig 5). These high intensity areas suggest changes in the structure or composition of the tissue, however they are a result of the dipolar nature of phase.

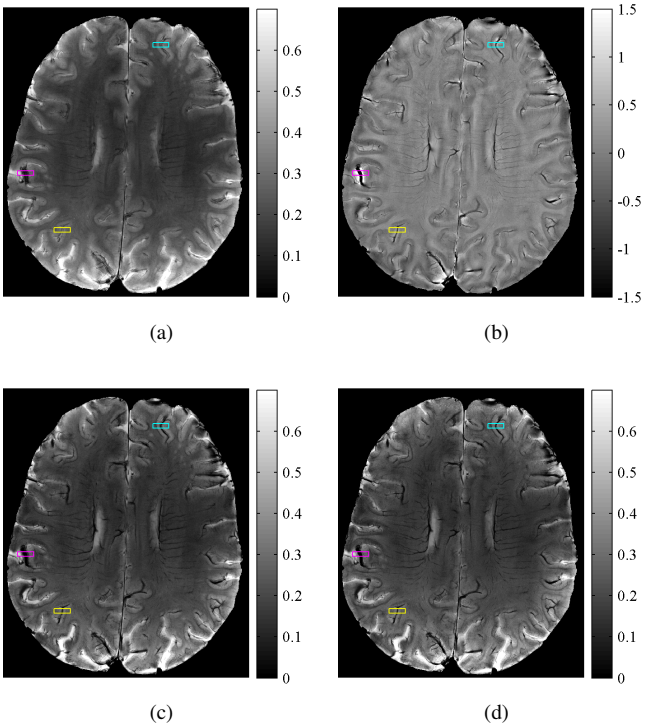

(a) (b) (c) (d)

Fig. 3: (a) Magnitude, (b) phase (in rads), (c) SWI and (d) sigmoid-SWI. ROIs are outlined in yellow, blue and pink. The main magnetic field is directed out of the page.

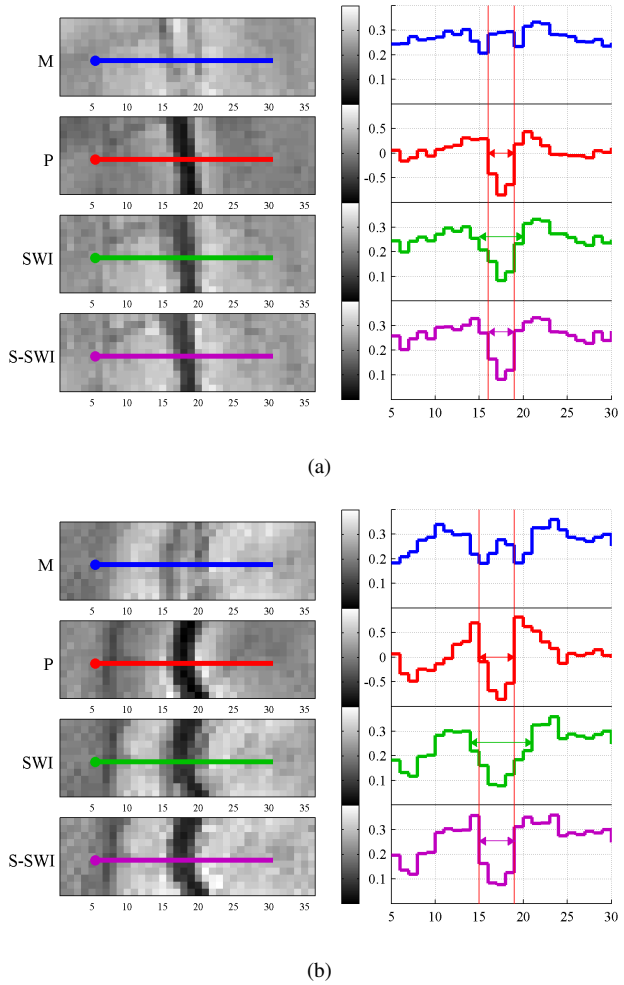

(a)

(b)

Fig. 4: Line profile comparisons for the (a) yellow ROI and (b) blue ROI outlined in Fig. 2. Line profiles are shown for (M) magnitude, (P) phase, SWI, and (S-SWI) sigmoid-SWI. Red vertical lines indicate the true boundary of the vessel, as delineated by phase information. Arrows in the line profiles indicate vessel width, derived as positions where the intensity crosses zero in the phase image and the mean intensity outside the vein in the SWI and sigmoid-SWI, as indicated by the vertical positioning of the arrows.

Inclusion of the threshold avoids these misleading artefacts and ensures recognisable contrast akin to conventional SWI.

The effectiveness of sigmoid-SWI is limited in situations where the absolute change in B field is large enough that phase differences greater than π occur between adjacent voxels. An example of this is demonstrated in Fig. 6. In the raw phase data, these shifts wrap to produce a phase difference less than π (light blue arrows), thus obscuring the true location of the large phase difference. Determining the positioning of these shifts is one of the difficulties faced by phase unwrapping algorithms. Information can sometimes be gathered from the magnitude, where an assumption is made that the structures that have differing magnetic susceptibility properties also have different relaxation properties, and their boundaries can therefore be determined by changes in

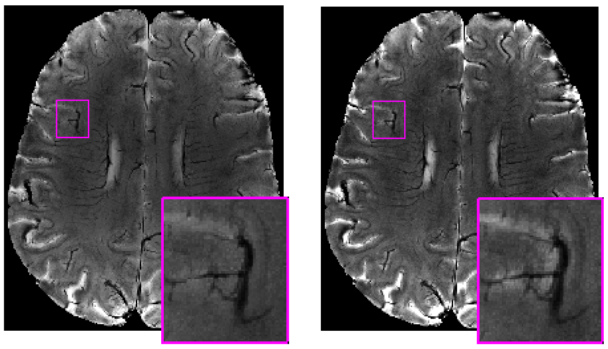

(a) (b)

Fig. 5: Comparison of (a) sigmoid-SWI using threshold, ρ_t, and (b) sigmoid-SWI with no thresholding (ie $\rho_t = \infty$)

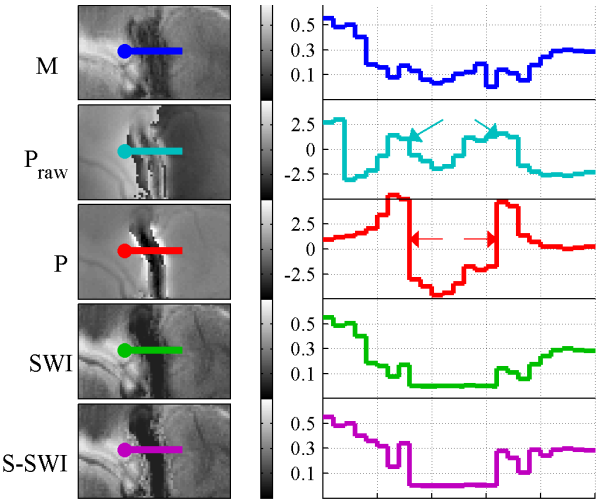

Fig. 6: Line profiles for the pink ROI in Fig (3). The (M) magnitude image shows low signal and SNR in the vicinity of the large vein. The (P_{raw}) raw phase image is wrapped such that true phase gradients greater than π appear as small phase shifts (light blue arrows). The determination of the location of these gradients (red arrows) in the (P) unwrapped phase image dictates the vessel boundaries and directly effects the results in the (SWI) susceptibility-weighted image and the (S-SWI) sigmoid-SWI image.

magnitude intensity. This assumption is normally valid in the case of veins bordering grey or white matter, as the T_2^* contrast has been demonstrated to increase with higher field strengths [4]. However, if the changes in the B field are large enough, the magnitude signal and signal-to-noise ratio (SNR) can decrease to a level where structural information is indistinguishable from noise and the assumption is no longer valid, as is demonstrated in Fig. 6. In this example, the estimated location of the large phase gradients and thus the vessel width cannot be validated, given the low magnitude signal. The estimation results in zero intensity voxels in the SWI and sigmoid-SWI where the vessel is deemed to be located. Non-vessel voxels located near the vessel boundary are attenuated in the SWI image and demonstrate amplified intensity in the sigmoid-SWI image. Since the magnitude intensity and SNR of these voxels is very low, the sigmoid-SWI method has amplified the noise. Translation of the vessel boundaries from the unwrapped phase to the sigmoid-SWI image still occurs, and therefore the effectiveness of the sigmoid-SWI method in delineating the vessels in these situations relies on the accuracy of the phase unwrapping method used.

V. Conclusions and Future Works

In this paper we have demonstrated that while SWI clearly shows the location of veins, the vein boundaries are blurred in larger vessels due to the attenuation in the magnitude image. Our proposed sigmoid-SWI technique successfully corrects the delineation of the veins, while preserving SWI values within the vessel. We therefore advocate use of sigmoid-SWI in place of conventional SWI processing for venography studies at high field strengths.

References

[1] E. M. Haacke, Y. Xu, Y. N. Cheng, and J. R. Reichenbach, "Susceptibility weighted imaging (SWI)," *Magnetic Resonance in Medicine*, vol. 52, no. 3, pp. 612–618, 2004.

[2] J. Reichenbach, R. Venkatesan, D. Schillinger, D. Kido, and E. Haacke, "Small vessels in the human brain: MR venography with deoxyhemoglobin as an intrinsic contrast agent," *Radiology*, vol. 204, no. 1, pp. 272–277, Jul. 1997.

[3] J. Budde, G. Shajan, J. Hoffmann, K. Uğurbil, and R. Pohmann, "Human imaging at 9.4 T using T_2*-, phase-, and susceptibility-weighted contrast," *Magnetic Resonance in Medicine*, vol. 65, no. 2, pp. 544–550, 2011.

[4] P. Koopmans, R. Manniesing, W. Niessen, M. Viergever, and M. Barth, "MR venography of the human brain using susceptibility weighted imaging at very high field strength," *Magnetic Resonance Materials in Physics, Biology and Medicine*, vol. 21, no. 1, pp. 149–158, 2008.

[5] E. M. Haacke, R. W. Brown, M. R. Thompson, and R. Venkatesan, *Magnetic resonance imaging: physical principles and sequence design*. New York: John Wiley & Sons, Inc, 1999.

[6] W. M. Spees, D. A. Yablonskiy, M. C. Oswood, and J. J. Ackerman, "Water proton MR properties of human blood at 1.5 Tesla: Magnetic susceptibility, T1, T2, T_2*, and non-Lorentzian signal behavior," *Magnetic Resonance in Medicine*, vol. 45, no. 4, pp. 533–542, 2001.

[7] A. Deistung, A. Rauscher, J. Sedlacik, J. Stadler, S. Witoszynskyj, and J. R. Reichenbach, "Susceptibility weighted imaging at ultra high magnetic field strengths: Theoretical considerations and experimental results," *Magnetic Resonance in Medicine*, vol. 60, no. 5, pp. 1155–1168, 2008.

[8] Z. Chen, L. A. Johnston, D. H. Kwon, S. H. Oh, Z. Cho, and G. F. Egan, "An optimised framework for reconstructing and processing MR phase images," *NeuroImage*, vol. 49, no. 2, pp. 1289–1300, Jan. 2010.

[9] S. Witoszynskyj, A. Rauscher, J. R. Reichenbach, and M. Barth, "Phase unwrapping of MR images using [Phi]UN - a fast and robust region growing algorithm," *Medical Image Analysis*, vol. 13, no. 2, pp. 257–268, Apr. 2009.

[10] A. Ng, L. Johnston, Z. Chen, Z. Cho, J. Zhang, and G. Egan, "Spatially dependent filtering for removing phase distortions at the cortical surface," *Magnetic Resonance in Medicine*, 2011. [Online]. Available: http://onlinelibrary.wiley.com/doi/10.1002/mrm.22825/abstract

[11] T. Chan and L. Vese, "Active contours without edges," *Image Processing, IEEE Transactions on*, vol. 10, no. 2, pp. 266–277, 2001.